JOURNAL OF THERMOPHYSICS AND HEAT TRANSFER
Vol. 15, No. 1, January–March 2001

Calculation of Nonequilibrium Radiation from a Blunt-Body Shock Layer

Takeharu Sakai* and Keisuke Sawada†
Tohoku University, Sendai 980-8579, Japan

A numerical method is developed for calculating the radiating axisymmetric flowfield accounting for nonequilibrium thermochemistry. Solutions of the flow with radiation are obtained in a fully coupled manner using a fully implicit time-marching method through a full block-matrix inversion. The method is used in calculating the radiation from the blunt-body shock layer in both air and carbon-containing airflows. The calculated results are compared with the experimental data obtained in a ballistic range at flight speeds of up to 13.4 km/s. For aluminum models, which do not ablate, the experimentally observed spectral features are qualitatively reproduced by the calculation, which assumes the shock layer to contain only the air species. For polycarbonate models, which ablate, additionally carbonaceous species must be included in the calculation in order to bring about qualitative agreement. Quantitative agreement is obtained for the ablating models only by accounting additionally for a blackbody radiation, produced possibly by spalled carbon particles.

Nomenclature

n_i = number density of species i, cm^{-3}
q_r = wall-ward radiative heat flux at the stagnation point integrated from 750 to 15,000 Å, W/cm^2
q_{rw} = wall-ward radiative heat flux at the stagnation point integrated from 2200 to 8500 Å, W/cm^2
T = translational temperature, K
T_v = vibrational temperature, K
κ_λ = absorption coefficient at given wavelength including stimulated emission, cm^{-1}
ρ = density, kg/cm^3
ρ_0 = sea-level atmospheric density
σ_λ = absorption cross section at given wavelength, cm^2

Subscripts

λ = wavelength, μm
∞ = freestream

Introduction

A NUMBER of planetary-Earth return missions are presently being planned, and some will be launched in the near future. Well-known examples are the Stardust mission[1] being carried out by the U.S. and the MUSES-C mission[2] planned by Japan. When the space vehicles enter into the Earth's atmosphere on return from such missions, the absolute velocity of the vehicle becomes typically 12.5 km/s at an altitude of 100 km. In these high-speed environments a significant portion of the heat-flux incident on the heatshield wall will be by radiation because the temperature in the shock layer over the vehicle becomes sufficiently high to produce strong radiation. The radiation in turn can affect the flow properties. Therefore, it is desirable to calculate the flowfield accounting for the radiation-flow coupling phenomenon.

Such a strong radiating flowfield is believed to have occurred for Apollo,[3] Pioneer-Venus,[4] and Galileo missions.[5] These missions yielded information on the heating environment and thermal response of the heatshield. The flight data for both Pioneer-Venus and Galileo showed higher heating rates at the frustum than at the stagnation point, which are different from the predictions.[6,7] Two different explanations were offered. In one, the ablating-product gas or the spalled carbon particles ejected from the heatshield enhances turbulence in the boundary layer near the frustum region.[8,9] In the other, the spalled particles increase the heat-transfer rate by nonequilibrium radiation of carbonaceous species in the shock layer.[10] How accurate these explanations are is yet uncertain. Any numerical calculation, which can account for these phenomena, will be worthwhile in this endeavor to identify the exact cause.

One difficulty in calculating such an environment is in the calculation of radiation. To calculate the radiation in these entry environments accurately, a large number of wavelength points is needed because absorption coefficients of a gas strongly depend on wavelength. Although a line-by-line method can calculate the radiation accurately, the method is very time-consuming and, therefore, not suited for the radiation-fluid coupling calculation. Radiative transport occurs over large distances, and this aspect of the phenomenon must be accounted for correctly in the coupling calculation. Because the expression of the radiative source includes a spatial integration of radiative properties, the conservation equations governing the flowfield become a set of nonlinear integro-differential equations.

Earlier, several multiband methods have been developed to reduce the computing time for radiation calculation.[11,12] These multiband methods use a few thousand wavelength points. The methods can reproduce a line-by-line calculation within a small error and reduce the computing time by a factor of 100. Attempts have been made to calculate a radiating flowfield with such multiband methods.[13,14] In Ref. 14 it is shown that the computing time becomes very large. To reduce the computing time, a totally novel approach is required.

A scheme named Planck–Rosseland–gray (PRG) model was developed to reduce the computing time for radiative transport calculation.[15] In this model the absorption coefficient at a given wavelength point at a given point in a flowfield is classified into one of the Planck, Rosseland, or gray-gas groups. The radiative heat fluxes are computed in each group, and the true value of the radiative heat flux is given by a sum of the radiative heat flux values in each of these three groups. This model successfully reduces the computing time of radiative transport by a factor of 10 compared with that by a multiband method and reproduces the calculation by using a line-by-line or multiband method within a small error. Using this new radiation model, a computer code for calculating a strongly radiating flowfield in thermochemical equilibrium has been developed.[16,17] The developed method was based on 1) multidimensional radiation

Presented as Paper 2000-0733 at the 38th Aerospace Sciences Meeting, Reno, NV, 10–13 January 2000; received 29 March 2000; revision received 1 August 2000; accepted for publication 23 August 2000.

*Research Fellow, Japan Society for the Promotion of Science, Department of Aeronautics and Space Engineering; currently NRC Associate, Mail Stop 230-2, Reacting Flow Environments Branch, NASA Ames Research Center, Moffett Field, CA 94035.

†Professor, Department of Aeronautics and Space Engineering. Senior Member AIAA.

calculation, 2) fully time-implicit integration, and 3) fully spatial coupling through inversion of a full loaded system of algebraic equations. The method has been applied for a strongly radiating shock-layer flow over a blunt body flying at a velocity of up to 16 km/s.

In Refs. 18 and 19 radiation emanating from the shock layer over a flying model was measured in a combined ballistic-range/shock-tunnel facility. The models were spherically nosed cylinders with 0.5-cm radius and 0.7-cm cylinder diameter and were made of either polyethylene, polycarbonate, or aluminum. The radiation was measured from the side-on view direction normal to the flight path. From the measured radiation intensities the radiation emissions per unit volume of shock layer were calculated. The radiative heat fluxes incident on the stagnation point were deduced from the emission values assuming an optically thin gas neglecting absorption by the boundary layer. The scatter in the radiative heat fluxes so determined was typically within a factor of 2.5.

In Ref. 17 the radiation coupled code has been tested for the experimental data.[18] The calculation was carried out only for the case of the flight velocity of 13.4 km/s because the assumption of thermochemical equilibrium was believed to be valid only for such high speeds. The result showed that the calculated radiative heat flux was lower than the measured value by a factor of at least four. At lower flight speeds radiation overshoot is known to occur in air behind the shock wave because of thermochemical nonequilibrium.[20] At 13.4 km/s such nonequilibrium radiation overshoot is not known to occur in pure air.[20] Whether such an overshoot can occur in air mixed with carbon is unknown.

The ultimate aim of the present study is to develop a computer code that can calculate the radiating nonequilibrium flowfield influenced by ablation and/or spallation. For this purpose the computer code developed earlier is extended to account for the nonequilibrium phenomena. By using the code, the calculation is carried out for the test conditions reported in Refs. 18 and 19.

Radiation-coupled calculation is performed for pure airflow first. The calculated total radiative heat flux at the stagnation point is found to be much lower than the measured values.

Two steps are taken to explain the cause of this discrepancy. First, cyanogen radical (CN) is included in the freestream, as was done in Ref. 17. CN is believed to have been produced by the interaction of spalled carbon particles with the airflow.[10] The comparison between the calculated spectra both for air and CN-laden airflow and the experimental spectra shows a fair agreement at the wavelength region below 5000 Å. At the wavelength region above 5000 Å, the calculation underestimates.

Second, to explain the discrepancy at wavelengths above 5000 Å the black-body radiation of the supposed spalled particles is added to the calculated spectra. This leads to a good agreement between the calculated and the measured spectra in the wavelength region above 5000 Å. The calculated and the measured radiative heat fluxes at the stagnation point for the ablating model agree fairly well also when CN and the blackbody radiation are both included.

Approach

In this study for pure air the nonequilibrium chemical state is described by 11 species (N, O, N_2, O_2, NO, N^+, O^+, N_2^+, O_2^+, NO^+, and e^-). For carbon-laden airflows an 18-species model (CO_2, N, O, C, N_2, O_2, NO, C_2, CN, CO, N^+, O^+, C^+, N_2^+, O_2^+, NO^+, CO^+, and e^-) is used. The nonequilibrium thermal state of the gas is described by a two-temperature model, where the vibrational and electron-electronic energy is governed by a common temperature. The governing equations are axisymmetric Euler equations, consisting of species mass-conservation equations, two momentum-conservation equations, a total energy-conservation equation, and a vibrational-electronic energy-conservation equation. Boundary layer is ignored here because the experimental values of radiative heat flux at the stagnation point[18,19] were obtained without considering a boundary layer, as was explained in the Introduction. The divergence of radiative heat flux is included in the right-hand side of the total and vibrational-electronic energy-conservation equations. Neglecting of the viscous phenomena results in underestimation of shock-wave thickness at low densities. This issue is discussed later in the General Features subsection. When solid particles exist in the flow, flow is disturbed. This problem is discussed in the Blackbody Radiation subsection.

The equation for vibrational-electronic energy conservation accounts for 1) vibrational energy excitation of molecules through collisions between heavy particles, 2) elastic energy transfer between electrons and heavy particles, 3) gains or losses of energy by electron impact ionization, 4) gains or losses of vibrational-electronic excitation energy of heavy particles in chemical reactions, and 5) energy loss by radiation. The preferential dissociation model is not used in this study. Vibrational relaxation parameter, such as vibrational relaxation times, are given by Refs. 20 and 21. The relaxation time accounts for Park's limiting cross section at high temperatures.[20,21]

The chemical kinetics model for high-temperature air is that proposed in Ref. 20 except that radiative recombination reactions are additionally included. For carbonaceous gas species a chemical kinetics model is not yet well defined, and therefore an 18-chemical kinetics model is developed. The values of reaction-rate coefficients are taken from Refs. 20 and 21 and are summarized in Table 1. In the two-temperature model thermal dissociation reactions occur by a geometrical average temperature $\sqrt{(TT_v)}$.

For radiative transport calculation the tangent-slab approximation is assumed to be valid. Radiative heat flux is calculated by the PRG model. A detailed explanation for the PRG model is presented in several papers.[15–17,22] A multiband model is used to determine the characteristic parameters needed in the PRG model. In the multiband model the absorption coefficients are evaluated at 2294 wavelength points for air and at 4060 wavelength points for carbonaceous species. They are constructed for the wavelength region from 750 to 15,000 Å. The absorption coefficient of the gas mixture is expressed as a sum of those for individual species in the form[11]

$$\kappa_\lambda = \sum_i n_i \sigma_{\lambda i} \tag{1}$$

where n_i is the number density of species i and $\sigma_{\lambda i}$ is the absorption cross section. The cross-section value is curve fitted using five parameters in the form[11]

$$\sigma_{\lambda i} = \exp\left(A^i_{\lambda 1}/z + A^i_{\lambda 2} + A^i_{\lambda 3}\ln z + A^i_{\lambda 3} z + A^i_{\lambda 5} z^2\right) \tag{2}$$

where $z = 10{,}000/T_v$. For air radiation N, O, N_2, O_2, NO, and N_2^+ are considered. For the carbonaceous gas species radiation C, C_2, CN, and CO are added.

The numerical method used is the finite volume method using the AUSM-DV scheme.[23] Spatial accuracy is improved by the MUSCL approach. The inviscid flux Jacobian is split by the conventional flux vector splitting technique. The Jacobian for the radiative source in the present nonequilibrium formulation is derived through a chain rule. The resultant implicit matrix has values in the off-diagonal terms. The system of linear algebraic equations is solved through a direct matrix inversion. A typical computational mesh (15×15 cells) is shown in Fig. 1. A calculation with a finer mesh (25×25 cells) was carried out in our previous study for similar problems.[17,22] According to the results of those studies, the radiative heat fluxes calculated with the computational mesh with 15×15 cells and those with 25×25 are indistinguishable. Therefore, all calculations are carried out by using the mesh with 15×15 cells in the present work.

The boundary conditions for the inviscid calculation are as follows: the boundary condition at the wall consists of a slip condition; a symmetry condition holds at the symmetry plane; the freestream condition is given at the inflow boundary; and the zeroth-order extrapolation is used at the outflow boundary. The boundary condition at the wall for the radiation-coupled calculation is that the wall is a blackbody of 2500 K.

Results and Discussion

General Features

In Figs. 2 and 3 the convergence history of the residual and wall-ward radiative heat flux at the stagnation-point wall, respectively, is shown for the case of flight velocity of 13.4 km/s and $\rho_\infty/\rho_0 = 10^{-4}$,

Table 1 Reaction-rate coefficients

Reaction	M	$k_f = CT_b^n \exp(-T_d/T_b)$, T_b	C	n	T_d	Source
		Dissociation reaction				
$N_2 + M \leftrightarrow N + N + M$	M_{mole}	$T^{0.5}T_v^{0.5}$	7.0^{21}	−1.6	113,200	Ref. 20
	M_{atom}	$T^{0.5}T_v^{0.5}$	3.0^{22}	−1.6	113,200	——
	e^-	T_v	1.2^{25}	−1.6	113,200	——
$O_2 + M \leftrightarrow O + O + M$	M_{mole}	$T^{0.5}T_v^{0.5}$	2.0^{21}	−1.5	59,500	——
	M_{atom}	$T^{0.5}T_v^{0.5}$	1.0^{22}	−1.5	59,500	——
$NO + M \leftrightarrow N + O + M$	M_{mole}	$T^{0.5}T_v^{0.5}$	5.0^{15}	0.0	75,500	——
	M_{atom}	$T^{0.5}T_v^{0.5}$	1.1^{17}	0.0	75,500	——
$C_2 + M \leftrightarrow C + C + M$	All	$T^{0.5}T_v^{0.5}$	3.7^{14}	0.0	69,900	Ref. 21
$CN + M \leftrightarrow C + N + M$	All	$T^{0.5}T_v^{0.5}$	2.5^{14}	0.0	71,000	——
$CO + M \leftrightarrow C + O + M$	M_{mole}	$T^{0.5}T_v^{0.5}$	3.4^{20}	−1.0	75,500	——
	M_{atom}	$T^{0.5}T_v^{0.5}$	2.3^{20}	−1.0	129,000	——
$CO_2 + M \leftrightarrow C + O + M$	M_{mole}	$T^{0.5}T_v^{0.5}$	6.9^{21}	−1.5	63,275	——
	M_{atom}	$T^{0.5}T_v^{0.5}$	1.4^{22}	−1.5	63,275	——
		Neutral exchange reaction				
$NO + O \leftrightarrow N + O_2$	——	T	8.4^{12}	0.0	19,450	Ref. 20
$N_2 + O \leftrightarrow NO + N$	——	T	6.4^{17}	−1.0	38,400	——
$CO + O \leftrightarrow C + O_2$	——	T	3.9^{13}	−0.18	69,200	Ref. 21
$CO + C \leftrightarrow C_2 + O$	——	T	2.0^{17}	−1.0	58,000	——
$CO + N \leftrightarrow CN + O$	——	T	1.0^{14}	0.0	38,600	——
$N_2 + C \leftrightarrow CN + N$	——	T	1.1^{14}	−0.11	23,200	——
$CN + O \leftrightarrow NO + C$	——	T	1.6^{13}	0.1	14,600	——
$CN + C \leftrightarrow C_2 + N$	——	T	5.0^{13}	0.0	13,000	——
$CO_2 + O \leftrightarrow O_2 + CO$	——	T	2.1^{13}	0.0	27,800	——
		Associative ionization reaction				
$N + O \leftrightarrow NO^+ + e^-$	——	T	8.8^{8}	1.0	31,900	Ref. 20
$O + O \leftrightarrow O_2^+ + e^-$	——	T	7.1^{2}	2.7	80,600	——
$N + N \leftrightarrow N_2^+ + e^-$	——	T	4.4^{7}	1.5	67,500	——
$C + O \leftrightarrow CO^+ + e^-$	——	T	8.8^{8}	1.0	33,100	Ref. 21
		Charge exchange reaction				
$NO^+ + O \leftrightarrow N^+ + O_2$	——	T	1.0^{12}	0.5	77,200	Ref. 20
$N^+ + N_2 \leftrightarrow N_2^+ + N$	——	T	1.0^{12}	0.5	12,200	——
$O_2^+ + N \leftrightarrow N^+ + O_2$	——	T	8.7^{13}	0.14	28,600	——
$O^+ + NO \leftrightarrow N^+ + O_2$	——	T	1.4^{5}	1.9	26,600	——
$O_2^+ + N_2 \leftrightarrow N_2^+ + O_2$	——	T	9.9^{12}	0.0	40,700	——
$O_2^+ + O \leftrightarrow O^+ + O_2$	——	T	4.0^{12}	−0.09	18,000	——
$NO^+ + N \leftrightarrow O^+ + N_2$	——	T	3.4^{13}	−1.08	12,800	——
$NO^+ + O_2 \leftrightarrow O_2^+ + NO$	——	T	2.4^{13}	0.41	32,600	——
$NO^+ + O \leftrightarrow O_2^+ + N$	——	T	7.2^{12}	0.29	48,600	——
$O^+ + N_2 \leftrightarrow N_2^+ + O$	——	T	9.1^{11}	0.36	22,800	——
$NO^+ + N \leftrightarrow N_2^+ + O$	——	T	7.2^{13}	0.0	35,500	——
$NO^+ + C \leftrightarrow NO + C^+$	——	T	1.0^{13}	0.0	23,200	Ref. 21
$CO + C^+ \leftrightarrow CO^+ + C$	——	T	1.0^{13}	0.0	31,400	——
$O_2^+ + C^+ \leftrightarrow O_2^+ + C$	——	T	1.0^{13}	0.0	9,400	——
		Electron impact ionization reaction				
$O^+ + e^- \leftrightarrow O^+ + e^- + e^-$	——	T_v	3.9^{33}	−3.78	158,500	Ref. 20
$N^+ + e^- \leftrightarrow N^+ + e^- + e^-$	——	T_v	2.5^{34}	−3.82	168,600	——
$C^+ + e^- \leftrightarrow C^+ + e^- + e^-$	——	T_v	3.9^{33}	−3.78	130,700	——

where ρ_0 is the standard atmospheric density. To investigate the strong coupling effect, the relaxation time between the translational and the vibrational mode is decreased by a factor of 100. From these figures one can infer that the flowfield is changed greatly when radiation is introduced. Though not shown, the change in flowfield causes substantial reduction in the shock stand-off distance and lowering of the two temperatures. The residuals decrease by more than two orders of magnitude within 200 iterations from the beginning of the coupled calculation for this case. The asymptotic value of the radiative heat flux is obtained within 100 iterations. For other cases convergence of the radiation-coupled solution is obtained within 200–1000 steps, depending on the allowed Courant–Friedrichs–Lewy number. The typical CPU time for one iteration requires 4, 17, and 54 s by using the equilibrium code developed earlier,[17] 11-species nonequilibrium air code, and 18-species nonequilibrium carbon-laden code, respectively. This increase of CPU time is caused mostly by the time expended for the direct matrix inversion. The codes run approximately at 1.2 Gflops on an SX-4 at the National Aerospace Laboratory in Kakuda, Japan.

Temperature profiles for pure airflow along the stagnation streamline for the cases of the flight velocity of 9.1 and 13.4 km/s and $\rho_\infty/\rho_0 = 10^{-4}$ are shown for the equilibrium and nonequilibrium calculations in Figs. 4 and 5, respectively. For both cases most of the shock layer is in a nonequilibrium state. One sees that the vibrational-electronic temperature is lower than the equilibrium temperature over the entire shock layer for the case of 13.4 km/s.

Figures 6–8 compare the calculated radiative heat fluxes reaching the wall at the stagnation point with experiments for the cases of the flight velocity of 6.1, 9.1, and 13.4 km/s, respectively. The radiative heat flux is evaluated over the wavelength range from 2200 to 8500 Å. It is seen that the values of the equilibrium radiative heat flux linearly decreases as the freestream density decreases for all

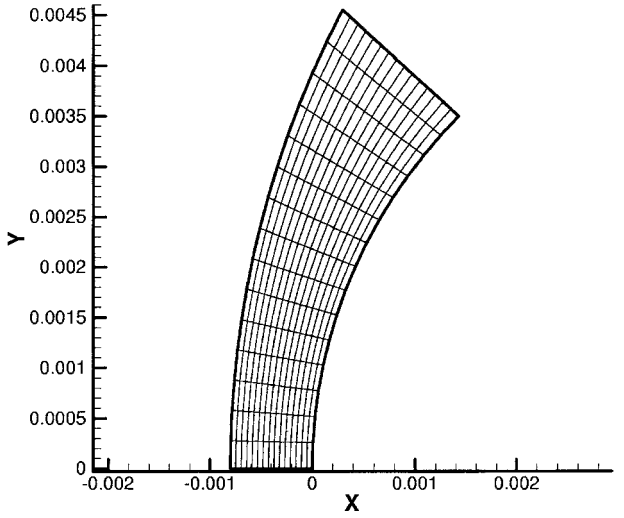

Fig. 1 Computational mesh (15 × 15 cells).

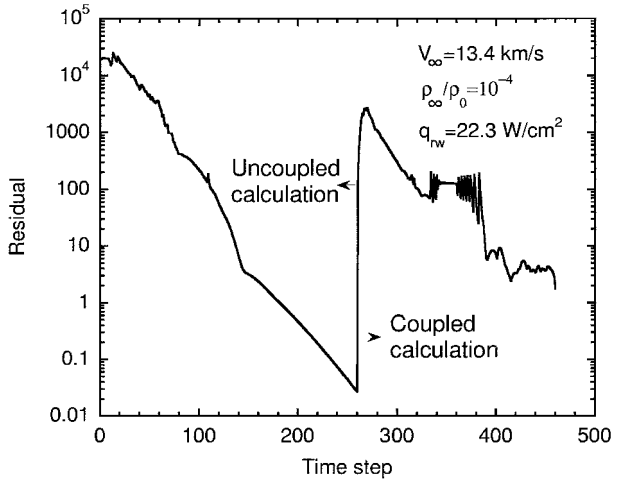

Fig. 2 Convergence histories for the case of the flight velocity of 13.4 km/s and $\rho_\infty/\rho_0 = 10^{-4}$. The relaxation parameter between the translational and the vibrational mode is reduced by a factor of 100.

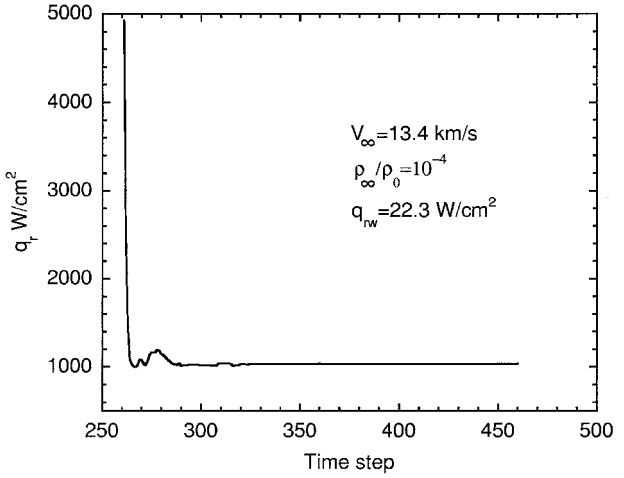

Fig. 3 Convergence histories for the wall-ward radiative heat flux at the stagnation point for the case of the flight velocity of 13.4 km/s and $\rho_\infty/\rho_0 = 10^{-4}$. The relaxation parameter between the translational and the vibrational mode is reduced by a factor of 100.

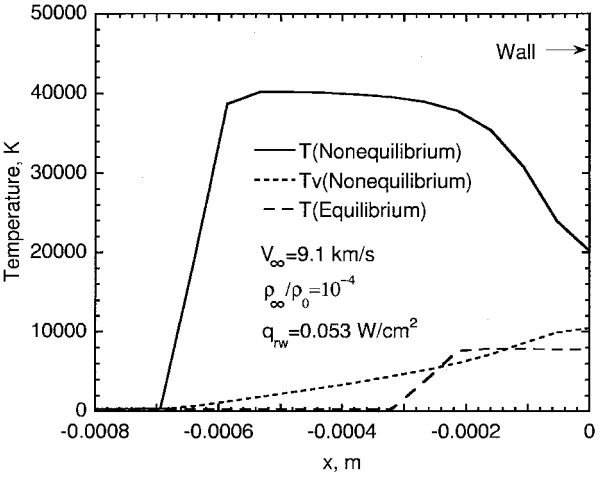

Fig. 4 Temperature profiles along the stagnation streamline for the case of the flight velocity of 9.1 km/s and $\rho_\infty/\rho_0 = 10^{-4}$ for equilibrium and nonequilibrium air cases.

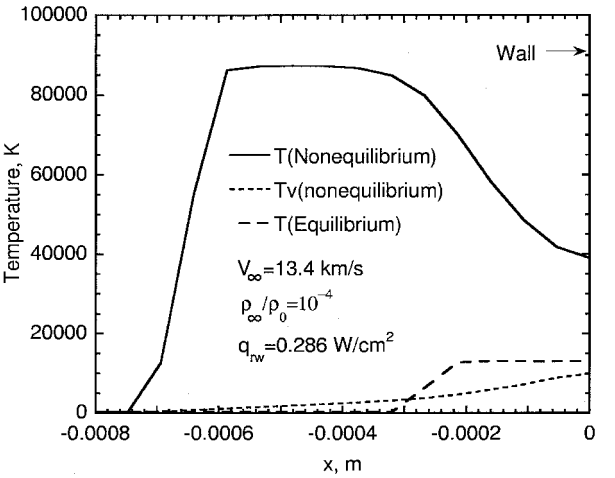

Fig. 5 Temperature profiles along the stagnation streamline for the case of the flight velocity of 13.4 km/s and $\rho_\infty/\rho_0 = 10^{-4}$ for equilibrium and nonequilibrium air cases.

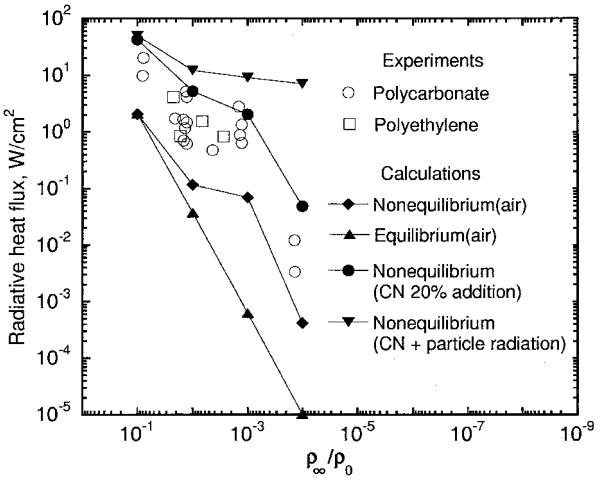

Fig. 6 Comparison of the calculated radiative heat flux at the stagnation point with the experimental data for the case of the flight velocity of 6.1 km/s.

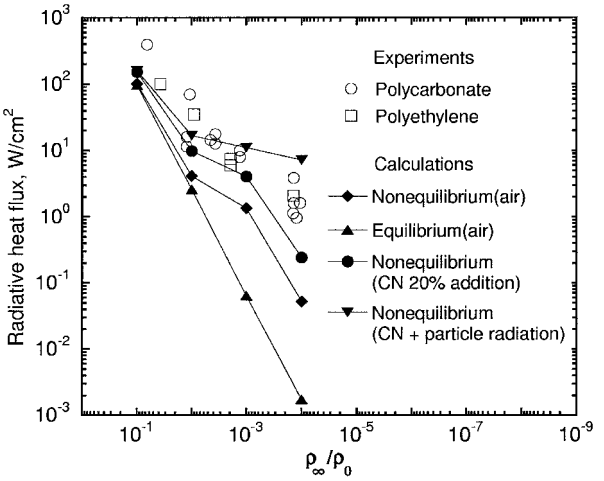

Fig. 7 Comparison of the calculated radiative heat flux at the stagnation point with the experimental data for the case of the flight velocity of 9.1 km/s.

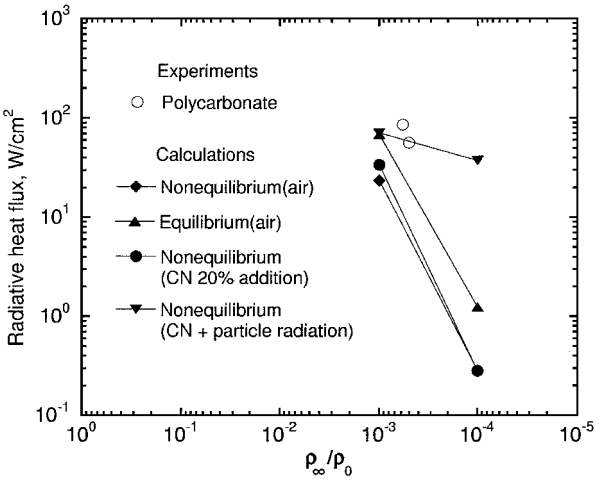

Fig. 8 Comparison of the calculated radiative heat flux at the stagnation point with the experimental data for the case of the flight velocity of 13.4 km/s.

calculated cases. For the cases of 6.1 and 9.1 km/s, the nonequilibrium radiative heat fluxes become higher than those for the equilibrium in the lower range of freestream density. This increase of radiation is known as radiation overshoot phenomenon. For the case of 13.4 km/s, the nonequilibrium radiative heat fluxes are lower than those of equilibrium. This is because the vibrational-electronic energy is low behind the shock, as is seen in Fig. 3. As a result, nonequilibrium radiation undershoots the equilibrium value, as reported in Ref. 19. Although the qualitative trend of the experimental data is reproduced by the nonequilibrium calculation, the calculated radiative heat flux values are lower than the experimental values by a factor of 10 over the entire freestream density.

The present calculation ignores viscosity. For the lower-density regime considered viscous phenomena may not be negligible. For the lowest density ($\rho_\infty/\rho_0 = 10^{-4}$) and highest velocity ($V_\infty = 13.4$ km/s) case, according to an unpublished viscous calculation (Gnoffo, P. A., private communication, Aug. 2000) for a sphere of the same nose radius as the present models, the boundary layer and the shock wave are merged, and the thickness of the shock wave is of the same order as the shock standoff distance obtained by the present inviscid calculation. The rise in vibrational temperature is slow, and its peak is about 4000 K. For this case the present inviscid calculation predicts a slow temperature rise to 8000 K at the wall. The radiation from the inviscid flow is higher than that from the viscous flow. However, viscous effects play a critically important role in determining the total radiation for the low-density case, particularly when interpreting the relative effects of CN and particle radiation for the lower densities in Figs. 7 and 8 shown in the following subsections.

CN Radiation

To test the hypothesis that the observed radiation is increased by the carbonaceous gas species produced by the interaction of air species with spalled particles,[10] 20% by mass of CN is added to the freestream arbitrarily. The choice of a 20% value will be explained later in the Blackbody Radiation subsection. The CN molecule was chosen for the carbonaceous species because it was found to be the main radiating species in the shock layer over an ablating model placed in an arc-jet wind-tunnel flow.[10] The coupled calculations with CN in the freestream are carried out for the velocities of 6.1, 9.1, and 13.4 km/s. For the purpose of comparing radiation spectrum, a line-by-line calculation was performed for the flowfield so calculated. A total of 500,000 wavelength points distributed at an equal photon energy interval was used for this calculation. The controlling temperature is taken to be the vibrational-electronic temperature.

In Refs. 18 and 19 spectral intensity distribution was measured using eight narrowband monochrometers. The average spectral emission power from a shock layer, in a unit of W/μ, was obtained in Ref. 18 by multiplying the measured spectral radiation power, in the units of W/μ-cm^3, by an effective radiating volume, denoted V_{eff}. To compare the present calculation with the experimental data, the calculated spectral emission power, in the units of W/μ-cm^3-ster, is multiplied by $4\pi V_{\text{eff}}$. Here, the value of V_{eff} is given as 0.00405 cm^3 (Ref. 19).

Figures 9 and 10 show the comparison of the spectral emission power between the computation and the experiment[19] for air and the CN-added case, respectively, for the case of flight velocity of 6.46 km/s and $\rho_\infty/\rho_0 = 0.019$. The difference between the air cases, Fig. 9, and CN-added case, Fig. 10, can be clearly seen over the entire computed wavelength range. The total radiative heat flux for the CN-added case is substantially higher (7.591 W/cm^2) than for the air case (0.322 W/cm^2). The calculation for air qualitatively reproduces the experimental values for the polyethylene and aluminum models. Although the polyethylene is also expected to ablate, the experimental spectrum for the polyethylene is almost identical to that for the aluminum model. One possible reason for this may be that the ablation rate of the polyethylene is relatively low. Another possibility is that aluminum models ablate, although weakly. The computed intensities for the CN-added case approach the experimental values for the polycarbonate model in the wavelength range of 4000–5000 Å, where the CN violet system is the major source of radiation. However, agreement is poor in the wavelength region above 5000 Å, regardless of the model material.

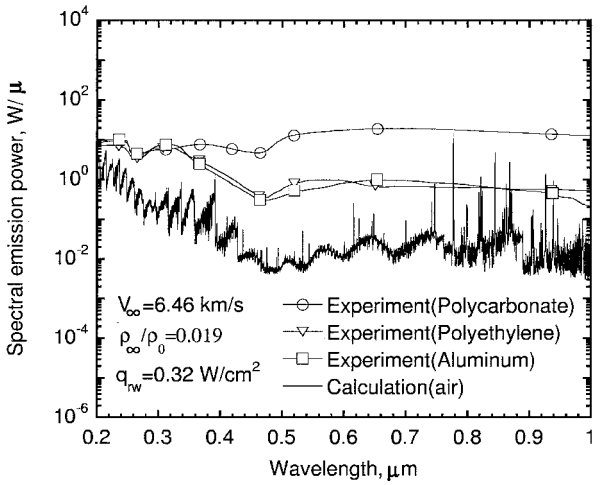

Fig. 9 Comparison of the calculated spectral emission power for air with the experimental data for the case of flight velocity of 6.46 km/s and $\rho_\infty/\rho_0 = 0.019$.

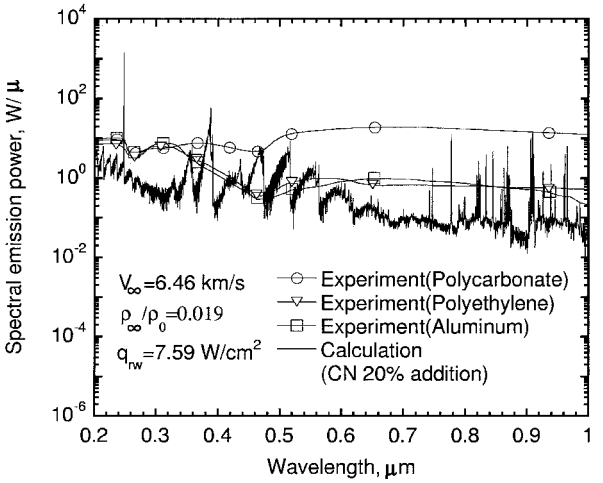

Fig. 10 Comparison of the calculated spectral emission power for the 20% CN-added case with the experimental data for the case of flight velocity of 6.46 km/s and $\rho_\infty/\rho_0 = 0.019$.

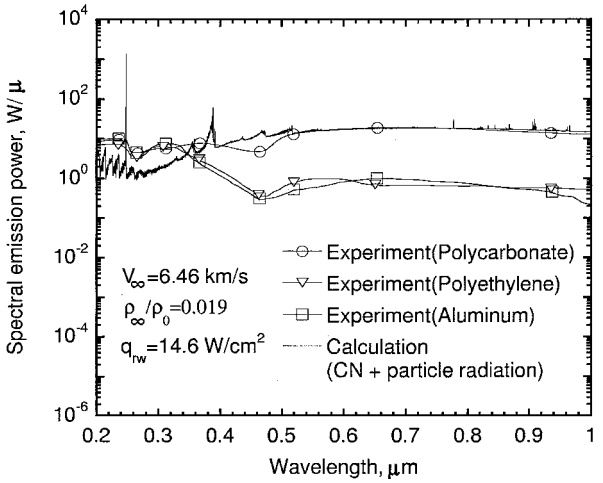

Fig. 11 Comparison of the calculated spectral emission power for the 20% CN-added and the blackbody-included case with the experimental data for the case of flight velocity of 6.46 km/s and $\rho_\infty/\rho_0 = 0.019$.

The stagnation-point radiative flux values calculated including CN are shown in Figs. 6–8. The calculation results in radiative heat-flux values that are a factor of about 1.5–100 larger for the cases of 6.1 and 9.1 km/s, in comparison with the nonequilibrium pure air data. One can see that generally fair agreement is obtained between the calculation and experiment, although the difference is large for the case of $\rho_\infty/\rho_0 = 10^{-4}$. The increase of the radiative heat-flux value by CN is suppressed for the case of 13.4 km/s. The temperature profiles along the stagnation streamline for this case are similar to those shown in Fig. 5 and, therefore, are not presented. The low vibrational-electronic temperature (Fig. 5) is the reason why radiative heat flux does not increase much for this case.

Blackbody Radiation

The preceding comparison shows two discrepancies between the CN-added calculation and the experimental data. First, even though the total radiation is closely reproduced by calculation, the intensities in the long wavelength range in the calculation are lower than the measured values (Figs. 9 and 10). Second, for the 13.4 km/s case the CN-added calculation results in heat-flux values substantially smaller than the measured values.

One possible reason for this discrepancy may be that the shock layer contains carbon particles, and they radiate as a blackbody. The polycarbonate and polyethylene models used in Ref. 18 could have produced spallation during their flight. Because such plastic materials contain carbon, the spalled particles will be mostly carbon. Because polycarbonate has a lower thermal conductivity than polyethylene, most likely it would have ablated more between the two. Aluminum should not have produced spalled particles. Reference 18 shows that the measured radiation was stronger with polycarbonate models than those made with either of the other two materials (see Figs. 9 and 10).

To explore the possibility that blackbody radiation by the spalled particles could produce the observed radiation, blackbody radiation of the solid particles is added in addition to CN in the calculation. The surface temperature of spalled particle was calculated in Ref. 8 for the environment of stardust-Earth reentry to be between 3700 and 4300 K. Therefore, the temperature is arbitrarily assumed here to be 4000 K. The blackbody spectrum is evaluated by multiplying the blackbody intensity, in the units of W/(μ-cm^2-ster), by $2\pi\beta_{\text{eff}}A_{\text{eff}}$, where β_{eff} denotes an effective surface factor, that is, the fraction of the 2π ster-radian solid angle covered by the particles, and A_{eff} is the effective radiating area given in Ref. 18. The value of A_{eff} is obtained as 0.23 cm^2. The value of β_{eff} is chosen arbitrarily as 0.03 to replicate the experimental spectrum. To obtain the stagnation-point radiative heat flux, the blackbody radiative heat flux is evaluated by multiplying the blackbody radiative heat flux integrated spectrally from 2200 to 8500 Å [W/(cm^2-ster)] by $\pi\beta_{\text{eff}}$. The value of β_{eff} is taken as 0.01 for the cases of 6.1 and 9.1 km/s and 0.02 for the cases of 13.4 km/s, respectively. The smaller values of β_{eff} are assumed for the stagnation point because the depth of the cloud of spalled particles is smaller when viewed from the stagnation point than when viewed from the side-on position in the experiment. The blackbody temperature is assumed arbitrarily to be 5000 K for the 13.4-km/s case.

The spectrum obtained including blackbody radiation is presented in Fig. 11. The spectrum was constructed by adding the blackbody spectrum to the gas spectrum, neglecting the interaction between the two. In reality, the solid particles partly block the gas radiation. The gas radiation is reduced by the mechanism to an order of β_{eff}. On the other hand, the radiation from the particles is partly absorbed by the gas. However, at wavelengths longer than 5000 Å, air absorption is weak. These considerations lead one to believe that simple sum of the two spectra will result in approximately the correct spectrum for the conditions of the present work.

As seen here, the spectrum in the experimental data obtained using the polycarbonate models above 5000 Å can be reproduced closely by the particle radiation. The radiative fluxes including the blackbody radiation are shown again in Figs. 6–9. As seen in these figures, agreement is good between the measured and the calculated values although the calculated radiative heat flux overestimates the experimental data for the case of lower flight velocities and lower freestream densities. Especially, for the case of 13.4 km/s, the heat flux becomes substantially higher than air and CN-added nonequilibrium calculation. The discrepancy at low densities is understandable: at low densities the amount of spallation will be less, and, therefore, the β_{eff} will be less. By using a smaller value of β_{eff}, it should be possible to reproduce the low-density data closely.

Because the β_{eff} value is of the order of 0.01, the ratio of the volume occupied by the particle to that gas will be of the order of 0.001. Because particulate density is typically 1000 times that of gas, mass of the particles in a unit volume will be of the same order as that of the gas. The effect of this large solid mass will affect the mass, momentum, and energy of the gas as follows:

1) The equation of conservation of gas mass must include a term representing the volume displacement by particles. The magnitude of that term is proportional to the volume ratio.

2) The equation of conservation of gas momentum must include a term representing the drag by the particles. The magnitude of that term is proportional to the area ratio β_{eff}.

3) The equation of conservation of gas energy must include a term representing the heat transfer between the particles and the gas. The magnitude of that term is also proportional to β_{eff}.

Because the β_{eff} and the volume ratio are small, the overall effect of the particles will be relatively small. In effect, the particles, though their total mass is large, merely slip through the gas without much interaction with the gas.

In the present calculations the value of 20% by mass of CN was used. Because the solid mass is of the same order as the gas mass, if 10% of mass of carbon particles is vaporized the concentration of atomic carbon produced will be equivalent to that of 20% CN.

The computed radiation intensities for the aluminum models are also lower than the experiment in the longer wavelength region. Whether this is caused likewise by particle radiation is unknown: There is as yet no evidence that spallation occurs to aluminum. If spallation occurs for aluminum, the experimental data for aluminum models can be explained also by the blackbody radiation of the spalled particles.

Concluding Remarks

An axisymmetric thermochemical nonequilibrium code is developed to simulate a radiating flowfield. This code solves the governing equations with radiation in a fully coupled manner through full block-matrix inversion. Radiative heat flux is evaluated by the PRG model. Two codes were written: one for pure air and the other for carbon-containing airflows. The codes reproduce the known radiation overshoot phenomenon at flight speeds below 10 km/s and the undershoot phenomenon at above 10 km/s. Compared with the experimental data obtained in a ballistic range, the radiative heat-flux values calculated for pure air are lower than the experimental values by a factor of at least 10. Spallation is accounted for by including CN molecules in the freestream and the blackbody radiation of the spalled particles. From the comparison of the calculated spectra with the measured spectra in the wavelength range below about 5000 Å: 1) the qualitative behavior of the experimental data for the nonablating body can be replicated by the airflow calculation, and 2) the qualitative behavior of those for the ablating body can be reproduced by the CN-laden airflow calculation. For the longer wavelength range above about 5000 Å: 1) the discrepancy for the nonablating body cannot be explained at present, and 2) most of the radiation observed for the ablating body is likely caused by spalled particles. For the spectrally integrated radiative heat flux the calculation reproduces the measured values fairly well by accounting for CN and the blackbody radiation.

Acknowledgments

The authors would like to thank Chul Park of NASA Ames Research Center, Moffett Field, California, for his helpful suggestions. The authors also would like to thank Peter A. Gnoffo of NASA Langley Research Center, Hampton, Virginia, for agreeing to use his calculations in the present paper. The present research has been supported by research fellowships of the Japan Society for the Promotion of Science for Young Scientists.

References

[1]Olynick, D., Chen, Y.-K., and Tauber, M. E., "Forebody TPS Sizing with Radiation and Ablation for the Stardust Sample Return Capsule," AIAA Paper 97-2474, June 1997.

[2]Ahn, H. K., and Park, C., "Preliminary Study of the MUSES-C Reentry," AIAA Paper 97-0278, Jan. 1997.

[3]Park, C., "Calculation of Real-Gas Effects on Blunt-Body Trim Angles," *AIAA Journal*, Vol. 30, No. 4, 1992, pp. 999–1007.

[4]Pitts, W. C., and Wakefield, R. M., "Performance of Entry Heat Shields on Pioneer Venus Probes," *Journal of Geophysical Research*, Vol. 85, No. A13, 1980, pp. 8333–8337.

[5]Milos, F. S., "Galileo Probe Heat Shield Ablation Experiment," AIAA Paper 96-1823, June 1996.

[6]Moss, J. N., Zoby, E. V., Sutton, K., and Anderson, E. C., "Aerothermal Environment for the Pioneer Venus Multiprobe Mission," *Aerodynamic Heating and Thermal Protection Systems*, Vol. 59, edited by L. S. Fletcher, Progress in Astronautics and Aeronautics, AIAA, New York, 1978, pp. 3–26.

[7]Moss, J. N., and Simmonds, A. L., "Galileo Forebody Flowfield Predictions," *Entry Vehicle Heating and Thermal Protection Systems: Space Shuttle, Solar Starprobe, Jupiter Galileo Probe*, Vol. 85, edited by P. E. Bauer and H. E. Collicott, Progress in Astronautics and Aeronautics, AIAA, New York, 1985, pp. 419–445.

[8]Ahn, H. K., Sawada, K., and Park, C., "CFD Calculation of Heat Fluxes in Turbulent Flow for Pioneer-Venus Probes," AIAA Paper 98-0833, Jan. 1998.

[9]Dendou, E., and Sawada, K., "Numerical Simulation of Hypersonic Flow over a Sphere with Surface Injection," AIAA Paper 98-0773, Jan. 1998.

[10]Park, C., "Interaction of Spalled Particles with Shock Layer Flow," *Journal of Thermophysics and Heat Transfer*, Vol. 13, No. 4, 1999, pp. 441–449.

[11]Park, C., and Milos, F. S., "Computational Equations for Radiating and Ablating Shock Layers," AIAA Paper 90-0356, Jan. 1990.

[12]Hartung, L. C., "Development of a Nonequilibrium Radiative Prediction Method for Coupled Flowfield Solutions," *Journal of Thermophysics and Heat Transfer*, Vol. 6, No. 4, 1992, pp. 618–625.

[13]Olynick, D. R., Henline, W. D., Chamber, L. H., and Candler, G. V., "Comparisons of Coupled Radiative Navier–Stokes Flow Solutions with the Project Fire II Flight Data," AIAA Paper 94-1955, June 1994.

[14]Gökçen, T., "Computation of Nonequilibrium Radiating Shock Layers," AIAA Paper 93-0144, Jan. 1993.

[15]Sakai, T., Sawada, K., and Park, C., "Assessment of Planck-Rosseland-Gray Model for Radiating Shock Layer," AIAA Paper 97-2560, June 1997.

[16]Sakai, T., Sawada, K., and Park, C., "Calculation of Radiating Flowfield Behind a Reflected Shock Wave in Air," *Journal of Thermophysics and Heat Transfer*, Vol. 13, No. 1, 1999, pp. 42–49.

[17]Sakai, T., Tsuru, T., and Sawada, K., "Computation of Hypersonic Radiating Flowfield over a Blunt Body," *Journal of Thermophysics and Heat Transfer*, Vol. 15, No. 1, 2000, pp. 91–98.

[18]Canning, T. N., and Page, W. A., "Measurements of Radiation from the Flow Fields of Bodies Flying at Speeds up to 13.4 Kilometers per Second," *The High Temperature Aspects of Hypersonic Flow*, edited by W. C. Nelson, Agardograph 68, Pergamon, New York, 1964, pp. 569–582.

[19]Page, W. A., and Arnold, J. O., "Shock Layer Radiation of Blunt Bodies at Entry Velocities," NASA TR R-193, April 1964.

[20]Park, C., "Review of Chemical-Kinetic Problems of Future NASA Missions. I: Earth Entries," *Journal of Thermophysics and Heat Transfer*, Vol. 7, No. 3, 1993, pp. 385–398.

[21]Park, C., Howe, J. T., Jaffe, R. L., and Candler, G. V., "Chemical-Kinetic Problems of Future NASA Missions. II. Mars Entries: a Review," *Journal of Thermophysics and Heat Transfer*, Vol. 8, No. 1, 1994, pp. 9–23.

[22]Sakai, T., "The Computation of Strongly Radiating Hypersonic Flowfields," Ph.D. Dissertation, Dept. of Aeronautics and Space Engineering, Tohoku Univ., Sendai, Japan, March 1999.

[23]Wada, Y., and Liu, M. S., "A Flux Splitting Scheme with High-Resolution and Robustness for Discontinuities," AIAA Paper 94-0083, Jan. 1994.